Progress In Electromagnetics Research M, Vol. 77, 83–92, 2019

Optimal Design of Beam-Deflectors Using Extended Unit-Cell Metagratings

Krupali D. Donda and Ravi S. Hegde*

Abstract—Recent reports on metasurfaces have focused on beam-deflector, a canonical optical element that can be used to compose other functionalities. Most reported designs, however, are limited to small deflection angles; large-angle ($\geq$ 50 degrees deflection) transmission-mode beam steering designs show poor efficiency. Furthermore, rapid efficiency degradation is observed for small deviations in the incidence angle. This paper presents a numerical study of beam-deflectors based on extended unit-cell metagratings (unit-cells containing multiple nanoantennae). In comparison to previous reports, the designs achieve significant efficiency improvements, wider acceptance angles and better polarization filtering. The versatility of the design technique is demonstrated by designing polarizing beam deflectors, polarization insensitive beam deflectors and prismatic beam deflectors.

1. INTRODUCTION

Metasurfaces, two dimensional arrays composed of periodic subwavelength sized meta-atoms, manipulate light by imparting local and space-variant changes on an incident wavefront [1, 2]. Nearly, all properties of electromagnetic waves like amplitude, phase, polarization, spectrum, etc. can be manipulated by the metasurface. This has motivated the design of metasurface based devices like the metalens [3], holograms [4], spectral filters [5] and vortex beam generators [6]. In addition to drastically shrinking the size, metasurfaces allow previously impossible functionalities like independent control of polarization components of the input beam. Dielectric metasurfaces can use conventional semiconductor materials like silicon and have gained much attention because of their low absorption loss (in comparison to plasmonic materials) and the possibility of leveraging state-of-the-art fabrication technologies.

While the constituent elements of a metasurface, the meta-atoms, are subwavelength resonators, the transverse extent of the metasurface can be several orders of magnitude larger than the operating wavelength (in other words, useful metasurfaces will be electrical large in the transverse plane). In general, the metasurface does not need to have any spatial ordering. The shapes of the individual meta-atoms, their positioning within the plane and their orientation are all free parameters. For heterogeneous metasurfaces, this means that the number of free parameters in the design of the metasurface can exceed 10^9 [7]. It is conceivable that the most optimal metasurface geometry for a particular task need not exhibit any convenient spatial ordering. However, the most general structure is not easily amenable for analysis and synthesis.

The simplest design technique, the so-called unit-cell approximation, is adopted in the conventional design of metasurfaces. The approximation refers to the fact that each constituent meta-atom is designed as if it was part of an infinite periodic lattice [7]. The approximation is justified in the limit that the neighbour interactions in a heterogeneous environment is similar to that in the periodic case. The

Received 28 September 2018, Accepted 10 December 2018, Scheduled 21 December 2018
* Corresponding author: Ravi S. Hegde (hegder@iitgn.ac.in).
The authors are with the Department of Electrical Engineering, Indian Institute of Technology-Gandhinagar, Gandhinagar, Gujarat 382355, India.

problem with this approach is that it tends to be inadequate in the presence of strong phase gradients, interactions between neighboring pillars, and large oblique incidence angles. These constraints become important for instance in the case of a focusing lens [7]. If periodicity is enforced on an extended scale that includes several individual resonator elements some of the limitations of the unit-cell approximation can be overcome. This technique is inspired by the Extended Local Periodicity (ELP) approach proposed for reflectarray design [8] in the field of RF antenna engineering. The metagrating, as proposed by Ra and coworkers [9], attempts to directly exploit the synergy between the highly directional scattering of individual nanoantenna as well as collective grating effects. The unit-cells in this configuration are still single-element, enabling analytical descriptions [10, 11]. The extended unit-cell metagrating, due to its size, also relies on the synergy between individual and collective effects but is not amenable to analytical descriptions.

In this paper, we describe a fast numerical optimization technique relying on global optimization methods and semi-analytical forward solvers that can serve as a clear design strategy for designing devices that exploit the synergy between individual and collective effects to realize performance goals. This paper builds on our recent preliminary reports [12, 13] and extends the work of Byrnes and coworkers [7] by replacing the local optimization techniques by more appropriate evolutionary optimization techniques. Specifically, we focus our attention to a beam deflector element which is a commonly used structure for bench-marking metasurfaces design strategies [7, 14] as the transmission efficiencies can be compared across designs. Several beam deflectors can be combined to produced metasurfaces with more advanced functionality like high numerical aperture and multi-wavelength focusing lenses and holograms [7, 14].

2. METHODOLOGY

2.1. The Extended Unit-Cell Metagrating and the Optimization Statement

Consider an extended unit-cell metagrating that lies parallel to the x-y plane with a thickness t. In this paper, we restrict our attention to metagratings with rectangular shaped unit-cells and elliptically shaped members as shown in Figure 1, so the unit-cell is specified by translation vectors $\mathbf{u_x}$ and $\mathbf{u_y}$. In each unit cell the number of nanoantennae N is limited by the condition: $N \leq P/d_{\min}$, where P determines the periodicity of the unit-cell and $d_{\min}$ is the minimum characteristic length of the nanostructure (this can be decided based on fabrication constraints). Each of the N elements (indexed

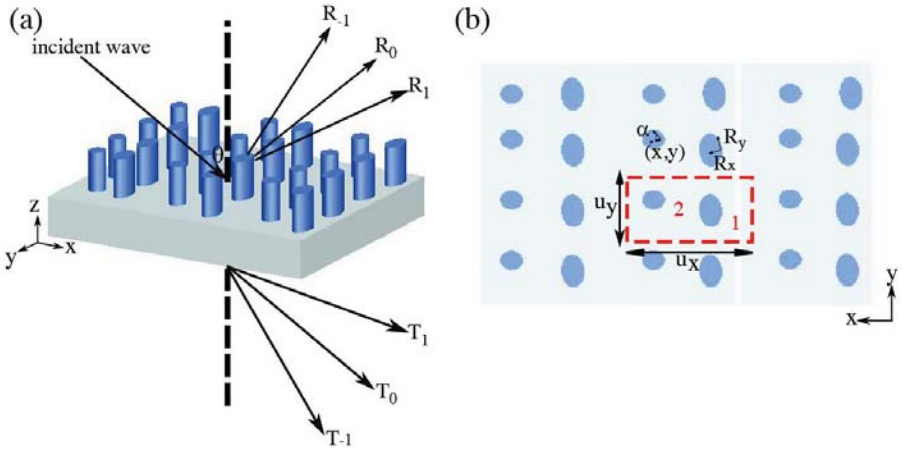

Figure 1. Schematic of the extended unit-cell metagrating with elliptically shaped members. (a) A plane wave is incident on it from the top and the propagation direction is characterized by the polar angle θ (w.r.t. z-axis) and an azimuth angle ϕ. The incident wave is then split into various reflection orders (R_0, $R_{\pm1}$, $R_{\pm2}$ and so on) and transmission orders (T_0, $T_{\pm1}$, $T_{\pm2}$ and so on). (b) Top-view of the metagrating with one extended unit-cell boundary shown in red. Inside each such cell, the N constituent members are numbered $1, 2, 3, \ldots, N$. For the i-th ellipse, the location is specified by x^i, y^i, the size by the axes lengths R_x^i and R_y^i and the orientation by the angle α^i.

as $1, 2, 3, \ldots, N$) is characterized by the location of its centroid, (x^i, y^i), an array of values characterizing its shape, $(s_1^i, s_2^i, \ldots)$ and an orientation angle, α^i.

A plane monochromatic wave is incident from the top and gets split into several reflection and transmission diffraction orders (by adding an optional reflecting layer behind the substrate, it is possible to cancel all the transmission orders). The incident plane wave can be characterized by its direction of incidence (characterized by the angle made by the propagation vector with the z axis by the pair of angles (θ, ϕ), it's polarization state (represented by the Jones vector $\mathbf{e}$) and its wavelength λ. The angles of the various orders is dictated by the period of the extended unit-cell and the efficiencies of the various orders is determined by the constituent members and the parameters of the incident wave. In this paper, we restrict our attention to linearly polarized waves and thus the polarization state can be specified using the TM and TE designation. If the polarization vector is parallel to the plane of incidence formed by the incident ray and the zeroth reflection and/or transmission orders it is designated as TM. Each transmission order is characterized by an index m, and the efficiency of diffraction into that order is denoted by η_t^m (the subscript r is used to denote a reflection order). This efficiency also depends on the incident polarization and thus we can add another superscript to the efficiency term, for example $\eta_t^{m,TE}$ would denote the efficiency of diffraction into the m-th transmission order under TE polarized illumination.

In the most general case, the optimization problem is to maximize the diffraction efficiencies of chosen reflection and/or transmission orders for specified ranges of incident wavelength, incident angles and polarization states, subject to obeying various constraints. Simultaneously, this could also require us to minimize the efficiencies of the remaining orders. These set of requirements can be encoded into a suitably designed cost function that is used in the optimization process. The first step is to decide on the range of values for the parameters of the incident wave like the wavelength (this is a set $\Lambda = \{ \lambda \mid \lambda_1 \leq \lambda \leq \lambda_2\}$) and incident angles (the sets $\Theta = \{ \theta \mid \theta_1 \leq \theta \leq \theta_2\}$ and $\Phi = \{ \phi \mid \phi_1 \leq \phi \leq \phi_2\}$). The set $\Omega = \Lambda \times \Theta \times \Phi$ which is the Cartesian set of these sets denotes the full range of the wave parameters. The set Ω can be then broken down into various subsets Ω_1, Ω_2 and so on ($\Omega = \Omega_1 \cup \Omega_2 \cup \ldots$). Over each of these parameter subsets, the various efficiencies of interest are calculated and averaged. For instance, the averaged m-th reflection order efficiency for TE-polarized incident wave in the parameter range set Ω_1 can be denoted as $\langle \eta_r^{m,TE} \rangle_{\Omega_1}$. The overall cost function can now be expressed as a weighted linear combination of these averaged efficiencies. The optimization problem can then be stated in the general form as:

$$\begin{aligned} \underset{s}{\text{maximize}} \quad & \sum_{i,m} \left(a_i^m \langle \eta_r^m \rangle_{\Omega_i} + b_i^m \langle \eta_t^m \rangle_{\Omega_i} \right) \\ \text{subject to} \quad & f_c(s) \leq con_i, \quad c = 1, 2, \ldots, C, \end{aligned} \tag{1}$$

where s denotes the vector of geometrical parameters of the extended unit-cell described above (location, size, orientation etc. of all the members), and the various a and b coefficients are decided based on the design specifications. Positive coefficient values will result in maximization of the efficiency of a particular order and negative coefficient will result in minimization. Fabrication techniques impose several constraints on realizable designs and these could be incorporated through C number of various functions f_c that describe constraints imposed on the values that the vector s or its elements can take. Some examples of the constraints are: (1) The size parameter of any member must be larger than a certain value which can be written as $s_i \geq l_d$, where l_d is the minimum feature size; (2) From considerations of aspect ratio, we can impose constraints like $s_i/t \geq R$, where R is the aspect ratio.

2.2. Implementation Details

The implementation details of the optimization procedure outlined above is summarized in the block diagram shown in Figure 2. The main component is the forward solver (in our implementation we use the Rigorous Coupled Wave Analysis (RCWA)) which takes the vector s and the incident wave parameters (direction, polarization state and wavelength) as input and gives the efficiencies of all the possible reflection and transmission orders as output. The RCWA is a semi-analytical method and can thus solve for the efficiencies must faster than full wave methods. We use the open-source software S_4 [15]

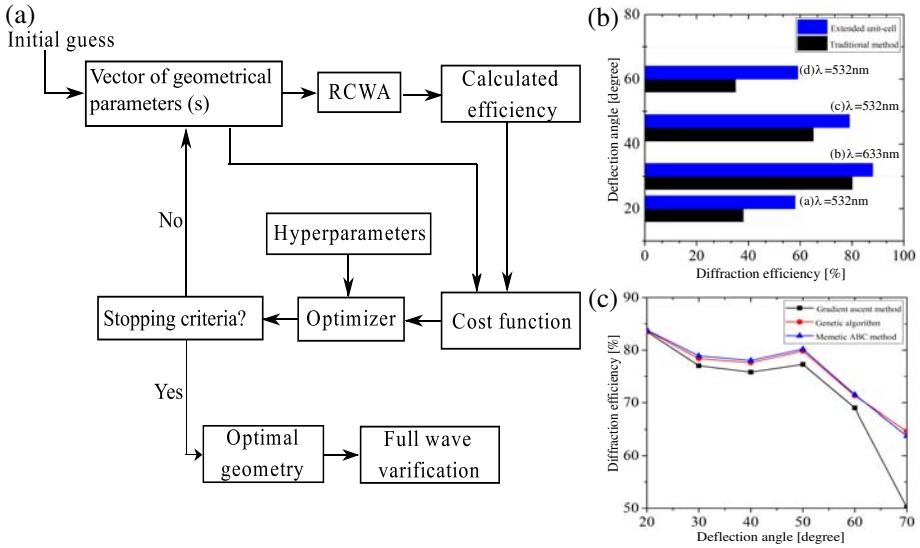

Figure 2. (a) Block diagram of the optimization procedure. (b) Comparison of diffraction efficiencies obtained using our extended unit-cell method (blue bars) with other simulation reports using traditional unit-cell method (black bars). (c) Comparison of the performance of our design methodology using local and global optimization.

which combines the S-matrix approach with the RCWA method. The number of RCWA modes is kept as 50. Full-wave simulations are performed using the commercial software program Lumerical FDTD. The full-wave FDTD solver and RCWA solver were able to independently reproduce the experimental results reported in [16, 17] and to reproduce the results for multiple-element unit-cells reported in [7]. As a final check, a full-wave solver is used to double check that the optimal solution does indeed generate the efficiencies as determined by the stopping criteria.

The second component is the optimization engine which uses the cost function and various constraints and updates the vector s. At each update, the stopping criteria are checked and, if they are met, the loop terminates and outputs an optimal s vector. Here we impose the condition that the minimum feature size of the entire shape should not be lower than 50 nm. Another physical constraint is to manage the aspect ratio. For instance, the best aspect ratio reported is 30 : 1 using deep reactive ion etching [18]. Our extended unit cell consists of two nanoellipses made of amorphous silicon ($n = 4.19$ at 520 nm) [19]. The height of nanopillars is kept as 550 nm.

In the optimizer, we have employed global optimization techniques. Due to the relatively large number of free parameters and stringent fabrication related constraints required to design efficient metasurface scanning over the full parameter space is not feasible, so, we have employed genetic and artificial bee colony algorithms. The ABC algorithm has achieved excellent results when solving continuous and combinatorial optimization problems. We have added memetic search phase to the ABC algorithm to further improve the search speed. The procedure to determine the correct hyper-parameters for the global optimization routines is reported earlier [12]. We have also released the full source code for this implementation, and it is available at [20].

3. RESULTS AND DISCUSSION

In this section, the design method outlined above is applied to a number of beam deflector design problems to show its versatility.

3.1. Large-Angle Polarizing Beam Deflectors

In previous reports of metasurface beam deflectors, the grating period was large, and efficiencies were limited especially for higher deflection angles. These metasurfaces have primarily demonstrated

functionality with plane waves at a normal incidence but, its diffraction efficiency dramatically decreases upon illumination with off-normal incidence angles. This is a major challenge for many optical applications where large range of acceptance angles, and uniform efficiency across the angular range is desired.

Using the extended unit-cell method, we have implemented large-angle beam deflectors which also have a wide acceptance angle (broad range of incidence angles). Figure 2(a) shows a comparison of efficiency figures of our design method with other published reports. First, we compare the efficiency figures for beam deflectors with various deflection angles reported by other workers. Four different designs were chosen: (a) 532 nm wavelength using amorphous silicon for 20° deflection angle reported by Zhenpeng and coworkers [21]; (b) 633 nm wavelength using amorphous silicon for 30° deflection angle reported by Daopeng and coworkers [22]; (c) 532 nm wavelength using amorphous silicon for 45° deflection angle reported by Daopeng and coworkers [22]; (d) 532 nm wavelength using TiO_2 for 60° deflection angle reported by Qing and coworkers [23]. Our designs using amorphous silicon were repeated keeping the same bend angle and wavelength and it is seen that the extended unit-cell provides significant improvements in efficiency. Figure 2(b) shows the advantages of using global optimization techniques in comparison to using simpler local search techniques [7]. This becomes evident especially at larger bend angles. Note that all these references are simulation based like our study.

For a sought deflection angle of θ_D at the incident wavelength λ_0, the period of the extended unit cell u_x is calculated using the equation,

$$u_x = \frac{\lambda_0}{\sin\theta_D}. \tag{2}$$

This assumes that the incident beam is primarily in the x-z plane thus allowing us to freely choose the other dimension u_y. For this design, the cost function discussed above will take the simpler form:

$$\begin{aligned} &\underset{s}{\text{maximize}} \quad \eta_t^{1,TM}(\lambda_D) \\ &\text{subject to} \quad f_c(s) \le con_i, \quad c = 1, \ldots, C. \end{aligned} \tag{3}$$

Although, we have chosen the +1-th transmission order here, it is entirely possible to use other orders.

We are designing metasurface which gives rise to a deflection angle of 50° upon normal incidence at a wavelength of 520 nm. The grating period of the unit cell is designed to be 678.81 nm as per Equation (2). The lateral period of cell is 400 nm. We set up the Genetic algorithm to maximize the diffraction efficiency in +1-th order at 520 nm. Minimum diameter and distance between pillars are set to be at least 50 nm for the fabrication constraint.

In Figures 3(a) and (b), the performance of the optimal design of the transmission mode beam deflector is shown for both polarization. The bending action at the designed angle for the TM polarization and TE polarization respectively can be seen. For the TE polarized illumination in Figure (b), it is observed that the wave is almost entirely reflected.

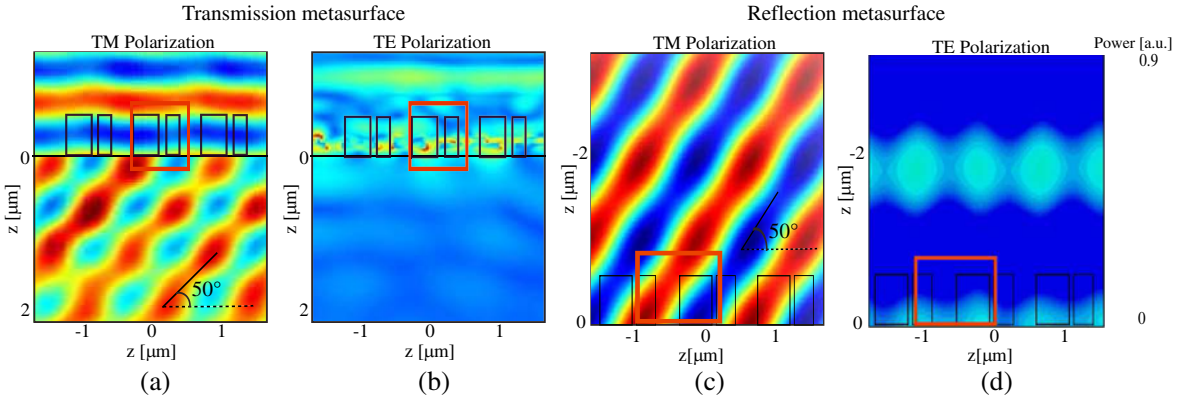

Figure 3. (Time-snapshot of the power flow in the near field for TM-polarization and TE-polarization incident waves for (a), (b) transmission metasurface and (c), (d) reflection metasurface respectively.

We have also designed a metagrating for working in reflection mode. The design principle of reflection metasurface is similar to transmission metasurface design with the addition of a reflecting layer (made of Aluminium) at the back of the substrate. The thickness of Al-layer is 100 nm and the thickness of the substrate is 500 nm. Al reflector at the bottom of the substrate prevent the light to transmit and reflect it back. so, in such metasurface it interacts with the nanoellipses twice. In Figures 3(c) and (d), shows the full wave plot of the near fields bending action at the designed angle for the TM-polarized and TE polarized beam of wavelength $\lambda = 520$ nm. The optimized nanoellipse-1 has x-radius = 180 nm, y-radius = 60 nm and it is oriented at angle 3° w.r.t. x-axes. Ellipse-2 has x-radius = 50 nm, y-radius = 70 nm, and it is oriented at angle −8° w.r.t. x-axes.

In Figures 4(a) and (b), the variation of the different efficiencies for the designed polarization and the orthogonal polarization are shown. These are compared with the simple unit-cell design reported in [17]. In order to have a fair comparison, the operational wavelength ($\lambda = 520$ nm), the material (amorphous silicon) and the deflection angle (50°) are kept the same for both designs. The design

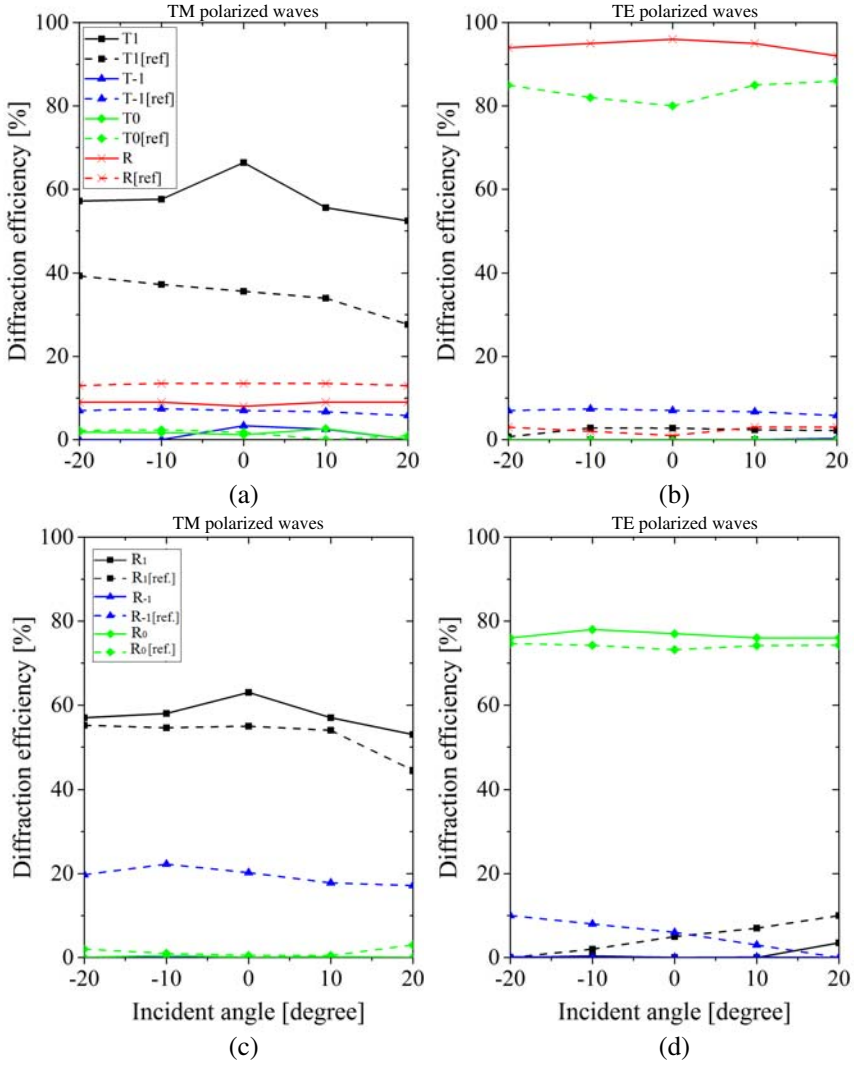

Figure 4. The variation of the efficiencies of different transmission and reflection orders as a function of the polar angle θ of the incident beam direction. (a) and (b) are for the transmission-mode metagrating. (c) and (d) are for the reflection-mode metagrating. (a), (c) are for TM-polarized incident wave while (b) and (d) are for TE-polarized incident wave. The curves shown in dotted line are obtained from reference [17].

reported by [17] is two dimensional and uses rectangular bars. The periodicity of their design was 380 nm and ours was 678.8 nm. As can be seen, the efficiency of the designed +1-th order in our design is well above 60% for both transmission and reflection mode designs. Also, it is seen to be nearly uniform for a broader range of incident angles θ. In contrast, their design shows a lesser average efficiency of only 35% for the transmission-mode. The efficiency is nonuniform and not changing in a symmetrical fashion (it is seen to be dropping as low as 29% for the transmission-mode). For the diffraction into unwanted other orders, efficiencies in our results are noticeably lower. For the orthogonal polarization, it is seen that the transmission is high in the 0-th order for their design, while in our case, it is reflected back almost entirely. Thus our design can achieve cleaner polarizing action.

A major consideration in the design of beam deflectors is the acceptance cone. Most designs typically consider normal incidence and see significant degradation in efficiency for slight deviations from normal incidence [17]. Figure 5 shows the variation of the efficiency of the optimal designs with changes in the direction of the the incident beam. Note that this design was carried out considering only the normal incidence and no explicit optimization was done to improve the acceptance angle. Also note that azimuthal angle in the range of 90 to 180 implies a reversal of the polarization and the efficiency is minimal in this range as expected. It is also expected that a gradual drop would happen from 0 to 90 degrees. Both the transmission-mode and reflection-mode designs exhibit gradual efficiency drop and are tolerant to changes in the incident wave direction. Figure S_1 and S_2 show the near-field power flow plots for off-normal incidence for the transmission-mode and reflection-mode optimal designs respectively. Because the design is two-dimensional in the case of Lin and coworkers [17], it is expected to be very sensitive to changes in the azimuthal angle unlike our design.

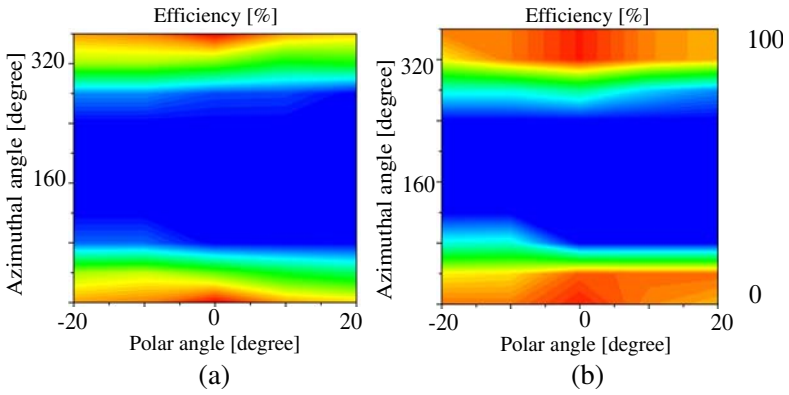

Figure 5. Efficiency plot for variation in polar angle and azimuth angle for (a) transmission metasurface (b) reflection mode metasurface for the incident of TM-polarized wave.

3.2. Polarization Insensitive Beam Deflectors

Most reports typically only report polarizing beam deflectors. Our method makes it possible to also design beam deflectors that is insensitive to polarization. For this design, the cost function discussed above will take the simpler form:

$$\begin{aligned} \underset{s}{\text{maximize}} \quad & \eta_t^{1,TM}(\lambda_D) + \eta_t^{1,TM}(\lambda_D) \\ & - w_f \left| \eta_t^{1,TM}(\lambda_D) - \eta_t^{1,TM}(\lambda_D) \right| \\ \text{subject to} \quad & f_c(s) \leq con_i, \quad c = 1, \ldots, C, \end{aligned} \tag{4}$$

where w_f denotes the weight factor. Typically the weight factor should be kept low during the initial searches and can be nudged up to fine-tune the design.

The optimal design unit cell has two elliptical members. The optimized nano ellipse-1 has x-radius = 117.55 nm, y-radius = 71.07 nm and it is oriented at angle 286.7° w.r.t. the x-axis. Ellipse-2 has x-radius = 69.57 nm, y-radius = 72.30 nm, and it is oriented at angle 36.8° w.r.t. the x-axis. A truly

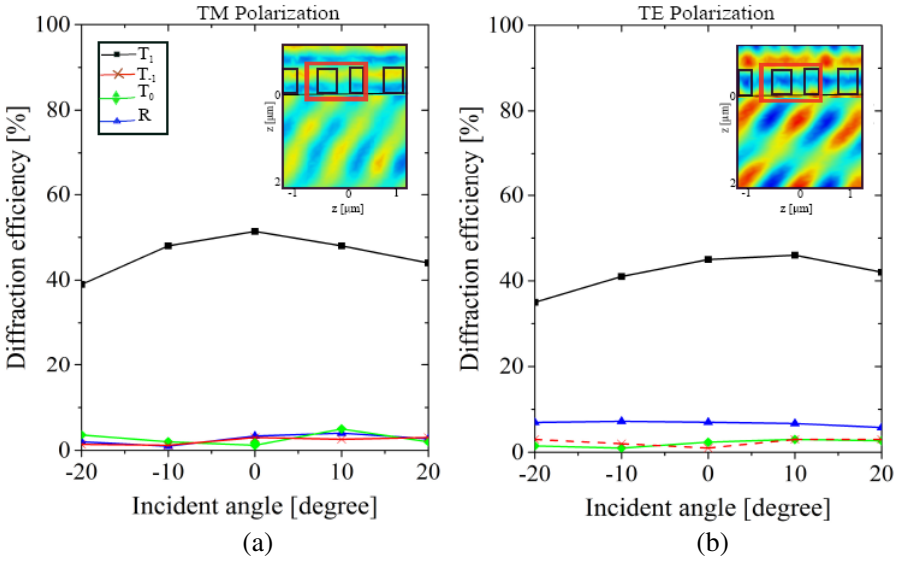

Figure 6. The variation of the efficiencies of different transmission and reflection orders for the polarization-insensitive metagrating as a function of the polar angle θ of the incident beam direction for (a) TM-polarized incidence, (b) TE-polarized incidence.

polarization insensitive design must exhibit a high degree of symmetry. It is seen that the optimal design does not exhibit such a high degree of symmetry. Figures 6(a) and (b), the full wave plot of the near fields show nearly identical bending action at the designed angle for both TE and TM polarizations. As can be seen in Figure 6, the curves are remarkably similar for both TE and TM cases. The TM case exhibits a slightly larger efficiency overall (difference of nearly 5% is observed).

3.3. Prismatic Beam-Deflectors

A prismatic metasurface splits an incoming white light beam so that different wavelengths are diverted into different bend angles (see Figure 7(a). Given a grating period u_x, the span in degrees for a range of wavelengths, $\lambda_{\min} \leq \lambda \leq \lambda_{\max}$, is given by:

$$\frac{180}{\pi} \arcsin\left(\frac{\lambda_{\max}}{u_x}\right) - \frac{180}{\pi} \arcsin\left(\frac{\lambda_{\min}}{u_x}\right). \tag{5}$$

For this design, the optimization problem can be stated in the form:

$$\begin{aligned} \underset{s}{\text{maximize}} \quad & \sum\nolimits_i \left\langle b_i^{1,TM} \eta_t^{1,TM} \right\rangle_{\Omega_i} \\ \text{subject to} \quad & f_i(s) \leq con_i, \quad i = 1, \ldots, C. \end{aligned} \tag{6}$$

In the above equation, the averaging is performed by first calculating the value of the efficiency at a number of discrete wavelength points, indexed by i, in the interval $\lambda_{\min} \leq \lambda \leq \lambda_{\max}$. The weights b can be used to gradually roll-off the efficiency, if desired.

We set our optimization algorithm to maximize how well light for the range 500–800 nm is deflected into the +1 diffraction order. The grating period is 848 nm which is calculated for the central wavelength 650 nm using Equation (2). Figure 7(b) shows the optimal geometry obtained. The simulated diffraction efficiency spectra of TM waves for metasurfaces with normally incident light in the wavelength range from 500 to 800 nm are shown in Figure 7(c). It is seen that the design manages to achieve an average efficiency of about 50% throughout the range. Amorphous silicon absorbs more towards lower wavelengths which explains the drop in efficiency observed at the lower wavelengths. The bending action of the designed metagrating is shown for the limits of the wavelength range 500 nm (see Figure 7(d)) and at 800 nm (see Figure 7(e)).

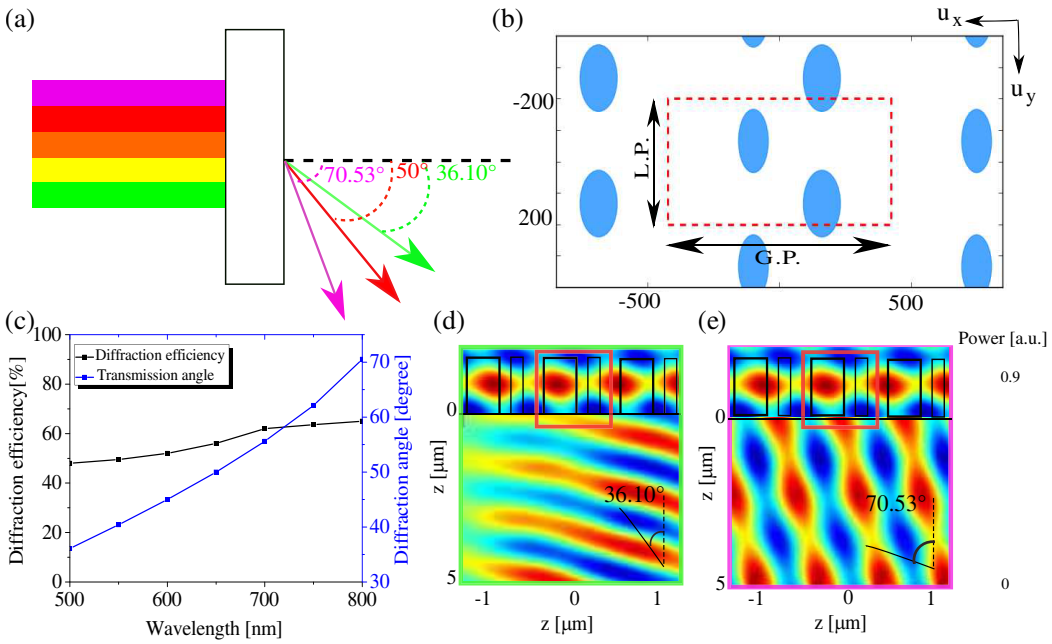

Figure 7. Design of a prismatic metasurface with wide span angle. (a) Shows the design goals with wavelength ranging from 500 nm to 800 nm and an achieved span of nearly 35°. (b) Shows the optimized geometry of the extended unit-cell. (c) Shows the achieved efficiency as a function of wavelength along with the bend angle. (d) and (e) show the time snapshots of the power flow in the near field for TM-polarized incident beam for incident wavelengths of 500 nm and 800 nm respectively.

4. CONCLUSION

In summary, we have presented a "brute-force" computational technique for designing metagratings with complicated multi-element unit-cells and shown the versatility of this design technique and the performance gains achievable. The article has focused on rectangular unit-cells and elliptically shaped member elements. We also focused here on linear polarization states and did not consider the design of birefringent metagratings. The proposed technique can be especially powerful in the design of chiral metagratings and birefringent metagratings. Inampudi and coworkers [24] have recently reported that neural networks can be a powerful technique for the design of metagratings. Their work has focused on single element metagratings. We are also working on applying neural network tools for designing extended unit-cell metagratings which could further speed up the search by indicating good starting geometries.

ACKNOWLEDGMENT

This work is supported by the Department of Science and Technology, Govt. of India through the Extramural grant SB/S3/EECE/0200/2015.

REFERENCES

1. Genevet, P. and F. Capasso, "Holographic optical metasurfaces: A review of current progress," *Reports on Progress in Physics. Physical Society (Great Britain)*, Vol. 78, No. 2, 24401, 2015.
2. Ding, F., A. Pors, and S. I. Bozhevolnyi, "Gradient metasurfaces: A review of fundamentals and applications," *Reports on Progress in Physics*, 81, 2018.
3. Khorasaninejad, M., W. T. Chen, R. C. Devlin, J. Oh, A. Y. Zhu, and F. Capasso, "Metalenses at visible wavelengths: Diffraction-limited focusing and subwavelength resolution imaging," *Science*, Vol. 352, No. 6290, 1190–1194, 2016.

4. Zheng, G., H. Mühlenbernd, M. Kenney, G. Li, T. Zentgraf, and S. Zhang, "Metasurface holograms reaching 80% efficiency," *Nature Nanotechnology*, Vol. 10, No. 4, 308–312, 2015.
5. Vashistha, V., G. Vaidya, R. S. Hegde, A. E. Serebryannikov, N. Bonod, and M. Krawczyk, "All-dielectric metasurfaces based on cross-shaped resonators for color pixels with extended gamut," *ACS Photonics*, Vol. 4, No. 5, 1076–1082, 2017.
6. Tang, S., T. Cai, G.-M. Wang, J.-G. Liang, X. Li, and J. Yu, "High-efficiency dual-modes vortex beam generator with polarization-dependent transmission and reflection properties," *Scientific Reports*, Vol. 8, No. 6422, 1–10, 2018.
7. Byrnes, S. J., A. Lenef, F. Aieta, and F. Capasso, "Designing large, highefficiency, high-numerical-aperture, transmissive meta-lenses for visible light," *Optics Express*, Vol. 24, No. 5, 5110, 2016.
8. Zhou, M., S. B. Sørensen, E. Jøgensen, P. Meincke, O. S. Kim, and O. Breinbjerg, "Analysis of printed reflectarrays using extended local periodicity," *Proceedings of the 5th European Conference on Antennas and Propagation*, 1494–1498, 2011.
9. Ra, Y., D. L. Sounas, and A. Alù, "Metagratings: Beyond the limits of graded metasurfaces for wave front control," *Physical Review Letters*, Vol. 119, No. 067404, 1–6, 2017.
10. Liu, W. and A. E. Miroshnichenko, "Beam steering with dielectric metalattices," *ACS Photonics*, Vol. 5, No. 5, 1733–1741, 2018.
11. Epstein, A. and O. Rabinovich, "Unveiling the properties of metagratings via a detailed analytical model for synthesis and analysis," *Physical Review Applied*, Vol. 8, No. 054037, 1–17, 2017.
12. Donda, K. D. and R. S. Hegde, "Rapid design of wide-area heterogeneous electromagnetic metasurfaces beyond the unit-cell approximation," *Progress In Electromagnetics Research M*, Vol. 60, 1–10, 2017.
13. Donda, K. D. and R. S. Hegde, "Evolutionary algorithms for designing metalenses," *IEEE International Conference on Microwave and Photonics (ICMAP 2018)*, 1–2, 2018.
14. Egorov, M. E. V. and J. Scheuer, "Genetically optimized all-dielectric metasurfaces," *Optics Express*, Vol. 25, No. 3, 2583–2593, 2017.
15. Liu, V. and S. Fan, "S4: A free electromagnetic solver for layered periodic structures," *Computer Physics Communications*, Vol. 183, No. 10, 2233–2244, 2012.
16. Yu, Y. F., A. Y. Zhu, R. Paniagua-Domínguez, Y. H. Fu, B. Luk'yanchuk, and A. I. Kuznetsov, "High-transmission dielectric metasurface with 2π phase control at visible wavelengths," *Laser and Photonics Reviews*, Vol. 9, No. 4, 412–418, 2015.
17. Lin, D., M. Melli, E. Poliakov, P. St Hilaire, S. Dhuey, S. Cabrini, M. Brongersma, and M. Klug, "Optical metasurfaces for high angle steering at visible wavelengths," *Scientific Reports*, Vol. 7, 1–8, 2017.
18. Yeom, J., Y. Wu, J. C. Selby, and M. A. Shannon, "Maximum achievable aspect ratio in deep reactive ion etching of silicon due to aspect ratio dependent transport and the microloading effect," *Journal of Vacuum Science & Technology B: Microelectronics and Nanometer Structures*, Vol. 23, No. 6, 2319, 2005.
19. Palik, E. D., *Handbook of Optical Constants of Solids*, Vol. 2, Academic Press, Boston, 1991.
20. "Github repository for metagrating design," https://github.com/rshegde/metasurfext, Accessed: Aug. 1, 2018.
21. Zhou, Z., J. Li, R. Su, B. Yao, H. Fang, K. Li, L. Zhou, J. Liu, D. Stellinga, C. P. Reardon, T. F. Krauss, and X. Wang, "Efficient silicon metasurfaces for visible light," *ACS Photonics*, Vol. 4, No. 3, 544–551, 2017.
22. Wang, D., Q. Fan, J. Wang, and Z. Zhang, "All dielectric metasurface beam deflector at the visible frequencies," *Opto-Electronic Engineering*, Vol. 44, No. 1, 103–107, 2017.
23. Zhang, Q., M. Li, T. Liao, and X. Cui, "Design of beam deflector, splitters, wave plates and metalens using photonic elements with dielectric metasurface," *Optics Communications*, Vol. 411, No. 596, 93–100, 2018.
24. Inampudi, S. and H. Mosallaei, "Neural network based design of metagratings," *Applied Physics Letters*, Vol. 112, No. 241102, 1–5, 2018.